THE JOURNAL OF PHYSICAL CHEMISTRY C

Article

pubs.acs.org/JPCC

Methane Storage in Metal-Substituted Metal–Organic Frameworks: Thermodynamics, Usable Capacity, and the Impact of Enhanced Binding Sites

Malay Kumar Rana, Hyun Seung Koh, Haroon Zuberi, and Donald J. Siegel*

Mechanical Engineering Department, University of Michigan, Ann Arbor, Michigan 48109, United States

Supporting Information

ABSTRACT: van der Waals density functional theory (vdW-DFT) and semiempirical grand canonical Monte Carlo (GCMC) calculations are used to predict the thermodynamics and methane storage capacity of 18 metal-substituted variants of the metal–organic framework (MOF) M-DOBDC (DOBDC = 2,5-oxidobenzene-1,4-dicarboxylate). Methane adsorption enthalpies (ΔH) on the benchmark Mg- and Ni-DOBDC systems were calculated using several vdW-DFT methods. The vdW-DF2 scheme was found to yield the best agreement with experiments, with a mean absolute deviation (MAD) of 2.7 kJ/mol. Applying this functional across the entire M-DOBDC series, it is observed that ΔH varies from −16 to −34 kJ/mol. These enthalpies are 10–20 kJ/mol less exothermic than that for CO_2 adsorption in M-DOBDC, consistent with a weaker, dispersion-based CH_4–MOF interaction. In parallel with these thermodynamic analyses, methane adsorption isotherms for five benchmark M–DOBDC MOFs were evaluated using several established interatomic potentials. An uncharged, single-site model for CH_4 yielded the best agreement with experiments, with a MAD of 16 cm^3/cm^3. This potential was subsequently employed to predict methane capacities across the remainder of the M–DOBDC series, with additional comparisons to other prominent MOFs such as MOF-5, PCN-11, PCN-14, and HKUST-1. Finally, the amount of *usable* stored methane was examined for two operating scenarios: isothermal pressure swing (PS) and a combined temperature/pressure swing (TPS). Under these conditions, PCN-11 and Be-DOBDC yield the best combination of gravimetric and volumetric methane densities at pressures below ∼50 bar, while MOF-5 is best at higher pressures. We conclude that enhanced binding sites, such as coordinatively unsaturated metal sites, can be detrimental for PS operation at higher pressures due to their tendency to retain adsorbed methane at low (desorption) pressures.

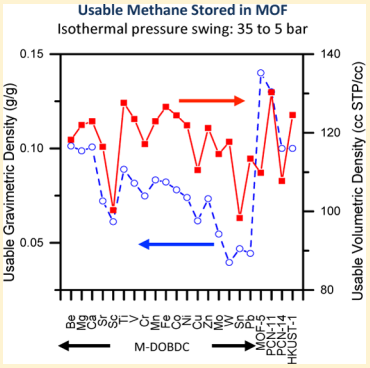

1. INTRODUCTION

Dramatic increases in the accessibility of natural gas (NG) reserves has sparked renewed interest in the use of NG as a vehicle fuel.[1] Adoption of NG vehicles (NGV) has been projected to reduce petroleum imports and CO_2 emissions from combustion within the transportation sector.[2] Nevertheless, the penetration of NGV remains limited, especially in the United States.[3] While a sparse refueling infrastructure has likely contributed to the slow adoption of NGV, the efficient on-board storage of NG also stands as an unresolved challenge.[1,4]

Methane (CH_4) comprises 70–90% of NG prior to refining, while refined NG distributed for home use consists almost entirely of CH_4.[5] As a gas at standard temperature and pressure (STP), the volumetric energy density of CH_4 is nearly 1000 times less than that of gasoline [0.0378 MJ/L (CH_4) vs 34.2 MJ/L (gasoline)].[6] Consequently, compression and liquefaction are commonly used to increase density. Since these approaches require compromises in efficiency, cost, and driving range/capacity, alternative strategies for achieving high-density storage of CH_4 are desirable.

Adsorbed natural gas (ANG) represents one such approach. In particular, hybrid inorganic–organic crystalline materials known as metal–organic frameworks (MOFs)[7−9] have recently emerged as promising high-capacity adsorbents for many gases,[10−13] including CH_4.[14−19] The high gas storage capacities of MOFs can be attributed to their permanent porosity, high surface area and pore volume, and tunable properties.[11] In comparison to hydrogen storage,[12,20] far fewer studies have examined CH_4 storage in MOFs.[19] Nonetheless, recent experiments have already identified a small number of MOFs with *total* CH_4 capacities in excess of 180 cm^3 (STP)/cm^3 at 298 K and 35 bar (which was the previous U.S. Department of Energy (DOE) storage target[1]). These include PCN-11 (181 cm^3/cm^3 [21]), M-DOBDC, with M = Mg, Mn, Co, Ni, and Zn (160–200 cm^3/cm^3 [22,23]), PCN-14 (195 cm^3/cm^3 [24]), and HKUST-1 (227 cm^3/cm^3 [24]). While these high capacities are clearly promising, they are far below the recently revised DOE targets of 349 cm^3/cm^3 and 0.5 g/g (materials basis, 298 K),[4] which refer to *usable* CH_4 available via a pressure swing between 35 and 5 bar (Table 1). Consequently, there is a clear need for new adsorbents with much higher CH_4 capacities. To

Received: October 21, 2013
Revised: January 13, 2014
Published: January 21, 2014

   dx.doi.org/10.1021/jp4104273 | J. Phys. Chem. C 2014, 118, 2929–2942

Table 1. U.S. Department of Energy Targets for Vehicular Natural Gas Storage[a4]

materials-level target		system-level target	
volumetric	gravimetric	volumetric	gravimetric
349 cm^3/cm^3	0.5 g/g	257 cm^3/cm^3	0.4 g/g
12.5 MJ/L	2.5 MJ/kg	9.2 MJ/L	2.0 MJ/kg
250 g/L		184 g/L	

[a]The targets are derived using a lower heating value of 50.0 MJ/kg, and refer to the usable capacity stored between 35 and 5 bar at near-ambient temperature.

accelerate the search for high-capacity MOFs, Wilmer et al.[25] used grand canonical Monte Carlo (GCMC) calculations to screen 137 953 hypothetical MOFs for their CH_4 capacities. Their screening identified the MOF NOTT-107[26] as having a methane storage capacity (213 cm^3/cm^3, total) slightly higher than the simulated uptake of PCN-14, the previous record holder.[27] In addition, nine other MOFs were predicted to have CH_4 capacities in the range 230−267 cm^3/cm^3.

While many features have been suggested to impact methane uptake in MOFs,[28,29] we note that essentially all of the high CH_4 capacity MOFs contain a combination of coordinatively unsaturated (metal) sites, CUS,[21−23,27] and deep-well "pocket" sites. (Throughout this article we will collectively refer to both CUS and pocket sites as "enhanced binding sites," EBS.) It has been argued that CUS result in relatively strong CH_4−MOF binding through enhanced Coulombic interactions,[30] while at the pocket sites comparable (or stronger) adsorption energies arise from enhanced van der Waals interactions.[22] Experiments have confirmed that CUS and pocket sites act as primary adsorption sites for CH_4;[22,30−32] thus, high volumetric capacities could be expected if these sites could be arranged in a high-density fashion. In addition, substitution of the CUS metal has been shown to dramatically alter the uptake of other small molecules such as CO_2,[33] suggesting a pathway for performance tuning. Nevertheless, EBS can also result in high uptake at low pressure,[22] resulting in a trade-off between high total capacities and reduced usable capacities during isothermal pressure swing desorption. Finally, CUS consisting of heavy transition metals will increase the MOF mass and thereby reduce the gravimetric storage density.

In light of the potential trade-offs associated with enhanced binding sites, in this study we examine the extent to which metal substitution at CUS impacts the thermodynamics and capacity for CH_4 adsorption in the prototype MOF, M-DOBDC (M_2(DOBDC) ($DOBDC^{4-}$ = 2,5-dioxido-1,4-benzenedicarboxylate), also known as MOF-74, CPO-27, and M_2(dhtp)). Experiments by Wu et al.[22] reported methane uptake in five metal-substituted M-DOBDC variants, where M = Mg, Mn, Co, Ni, and Zn, with high excess capacities ranging from 149 to 190 cm^3/cm^3. These measurements identified the CUS as the primary CH_4 adsorption site, with unusually large adsorption enthalpies approaching 20 kJ/mol. A recent reevaluation of these capacities found that Ni-DOBDC exhibits the highest total volumetric capacity for CH_4 of any experimentally tested MOF (228 cm^3/cm^3, at 298 K and 35 bar).[24]

In the present study we extend the composition range of the CUS by considering 18 metal-substituted variants of M-DOBDC, with M = Be, Mg, Ca, Sr, Sc, Ti, V, Cr, Mn, Fe, Co, Ni, Cu, Zn, Mo, W, Sn, and Pb. Our previous report[34] on the thermodynamic screening of M-DOBDC compounds demonstrated that some of these MOFs are promising for CO_2 capture, with predicted adsorption enthalpies (ΔH) falling within the desired thermodynamic window of −40 to −75 kJ/mol.[35] Taken together, these factors motivate us to consider the M-DOBDC series as candidate methane storage materials. To this end, a combination of van der Waals augmented density functional theory[36] (vdW-DFT) and semiempirical grand canonical Monte Carlo calculations are used to predict the thermodynamics and capacities for CH_4 uptake in the M-DOBDC series. In addition, we revisit the predicted capacities in other prominent MOFs, including MOF-5, PCN-11, PCN-14, and HKUST-1. Our hope—and the emerging trend[25]—is for computation to accelerate the search for promising methane adsorbents. Consequently, a portion of our study is devoted to assessing the accuracy of these methods by validating the predicted adsorption enthalpies and capacities with experimental data. These comparisons are timely because van der Waals density functionals are rapidly evolving,[37−39] and typical classical interatomic potentials do not always capture interactions with CUS.[30,40] Such comparisons provide an important benchmark as the field of CH_4 storage continues to grow.

Regarding the energetics of CH_4 adsorption, accurate thermodynamic data are important because these properties strongly impact the thermal behavior of a MOF-based methane storage system. An ANG system will release heat during uptake and potentially require heat input to bring about maximum desorption. Managing this heat exchange process will influence the efficiency, design, and cost of the storage device. Other factors being equal, a desirable methane adsorbent will have both a high capacity and a small enthalpy of adsorption.

Recent reports have shown that vdW-DF[39,41] can yield accurate estimates of the enthalpy of adsorption (ΔH) for H_2 and CO_2 in MOFs.[42−45] In the case of CO_2, the mean absolute deviation (MAD) between the calculated vdW-DF1[39] and experimental ΔH across several metal-substituted MOFs was only 3.4 kJ/mol.[34,43] A natural question is whether comparable accuracy can be attained for methane adsorption. In the present study we find that the rPW86-based vdW-DF2[41] method outperforms conventional (PBE-GGA[46]), semiempirical (DFT-D2),[38] and other vdW-based density functionals in predicting ΔH for CH_4. Agreement with experimental adsorption enthalpies is good, with a mean absolute deviation of 2.7 kJ/mol. In contrast to CO_2 adsorption, which exhibits relatively strong electrostatic interactions that are 10−20 kJ/mol more exothermic than for CH_4,[34,43] the dominant contribution for methane binding arises from weaker dispersion interactions.

Regarding CH_4 capacity, GCMC is the standard method for predicting CH_4 uptake in porous materials.[25,28] Nevertheless, the accuracy of these predictions are only as good as the interatomic potentials employed. Although earlier GCMC calculations have found good agreement with measured CH_4 isotherms at moderate temperatures and pressures,[47] more recent work has identified discrepancies with experiments at low temperatures and pressures[30,31] and in the location of preferred adsorption sites.[30] Herein we assess the sensitivity of the predicted uptake to the choice of interatomic potential by comparing six "off the shelf" CH_4−MOF potentials. The potentials differ in their description of the CH_4 molecule (single site[48,49] vs five sites,[50,51] charged vs uncharged) and in the parameters used to describe the MOF atoms (charged vs uncharged, UFF[52] vs DREIDING[53]). We find that a simple uncharged single-site model for CH_4 based on the TraPPE[48]

dx.doi.org/10.1021/jp4104273 | J. Phys. Chem. C 2014, 118, 2929−2942

potential yields CH_4 uptake in DOBDC in best agreement with experiments.

Finally, the optimal interatomic potential is used to predict CH_4 uptake across the remainder of the M-DOBDC series, and in other noteworthy MOFs (MOF-5, PCN-11/14, and HKUST-1) as a function of maximum operating pressure (P_{max}) and for three operating scenarios: (i) *total capacity* at 298 K; (ii) *usable capacity* at 298 K assuming a pressure swing between P_{max} and 5 bar; (iii) *usable capacity* assuming both a temperature and pressure swing from 298 K, P_{max}, to 358 K (85 °C), 5 bar. Although none of the studied compounds come close to achieving the DOE targets, we find that Be-DOBDC, PCN-11, and (surprisingly) MOF-5 provide the best combination of *usable* gravimetric and volumetric capacities. Importantly, the EBS-containing MOFs Be-DOBDC and PCN-11 perform best at pressures less than ∼50 bar; however, the presence of EBS is detrimental at higher pressures, where MOF-5 emerges as the best adsorbent. Moreover, the higher heat management requirements expected for EBS-containing MOFs (due to their larger ΔH) suggests that compounds without EBS should receive additional study as promising materials for CH_4 storage.

2. METHODS

Density Functional Theory. Methane adsorption energies were calculated using van der Waals augmented density functional theory,[36] as implemented in the VASP[54,55] code. For the M-DOBDC series, crystal structures measured by diffraction experiments for pristine Mg-DOBDC and CH_4-adsorbed Mg-DOBDC (loading of 1 CH_4 per metal site) were adopted as initial structural models.[22] The metal component (M) of DOBDC was then varied among elements having the potential to exhibit a +2 oxidation state,[34] including four alkaline earths: Be, Mg, Ca, Sr; 11 transition metals: Sc, Ti, V, Cr, Mn, Fe, Co, Ni, Cu, Zn, Mo, and W; and two group-14 metals: Sn and Pb. The computational cell of the empty MOF contained 54 atoms; six CH_4 molecules were added to represent the adsorbed state. The empty and CH_4-containing supercells both exhibit $R\bar{3}$ symmetry, as suggested by experiments.[22] All calculations were spin-polarized and assumed a ferromagnetic ordering. (Although antiferromagnetic ordering has been discussed for these systems,[56,57] test calculations on Fe, Co, and Ni-DOBDC revealed that the magnetic state has a negligible impact on the CH_4 adsorption energy: we find that ΔE changes by at most 0.2 kJ/mol upon varying the spin state.) A plane-wave cutoff energy was 500 eV; *k*-point sampling was performed at the Γ-point and yielded adsorption energies converged to better than 1 kJ/mol CH_4. (For density of states calculations a denser *k*-grid of 2 × 2 × 2 was used.) Interactions between core and valence electrons were described by the projector-augmented-wave (PAW) method[55] with semicore electrons treated as valence. The shape and volume of the MOF unit cells were optimized for each compound; in addition, atomic positions were relaxed to a tolerance of 0.01 eV/Å. Further details can be found in our prior publications.[34,43]

Static adsorption energies (ΔE) at 0 K were calculated using $\Delta E = (1/n)(E_{MOF+CH_4} - E_{MOF} - nE_{CH_4})$, where E_x refers, respectively, to the total energies of the MOF + CH_4 complex, the isolated MOF, and an isolated CH_4 molecule. n is the total number of adsorbed CH_4 molecules. Adsorption enthalpies at T = 300 K were calculated according to $\Delta H = \Delta E + \Delta E_{ZPE} + \Delta E_{TE}$, where the total enthalpy of a system is given by $H = E_0 + E_{ZPE} + E_{TE}$. Here E_0 is the 0 K static total energy and $E_{ZPE} = \sum_i \hbar\omega_i/2$ and $E_{TE} = \sum_i \hbar\omega_i/[\exp(\hbar\omega_i/k_BT) - 1]$ are the zero point energy and vibrational contributions. k_B is the Boltzmann constant, and ω_i are the normal mode vibrational frequencies which were evaluated using frozen phonon calculations at the gamma point of the first Brillouin zone. In the case of free CH_4, an additional 4 k_BT is added to E_{TE} to account for translational, rotational, and *PV* degrees of freedom.

Grand Canonical Monte Carlo. Grand canonical Monte Carlo (GCMC) calculations were used to predict CH_4 adsorption isotherms on the DFT-optimized MOF structures. An expanded 1 × 1 × 4 conventional cell with periodic boundary conditions was used as the simulation cell. All atoms associated with the MOF were kept fixed during the simulation. Interactions between CH_4 molecules, and between MOF atoms and CH_4, were described using a Lennard-Jones (LJ) potential, including an optional electrostatic term:

$$E(r) = D_o\left[\left(\frac{R_o}{r}\right)^{12} - 2\left(\frac{R_o}{r}\right)^{6}\right] + \frac{qq'}{r}$$

where D_o and R_o are the energy and distance LJ parameters, r is the distance between two interacting atoms, and q and q' represent partial charges on those atoms. LJ parameters for MOF atoms and for various CH_4 models (described below) are listed in Table S1 in the Supporting Information. For potentials involving electrostatic interactions, partial charges on the MOF atoms are assigned using the REPEAT method,[58] and the long-ranged Coulombic interaction was evaluated via an Ewald sum. The cutoff for atomic interactions was set at 12.5 Å, and a value of 10^{-5} kcal/mol was used for the Ewald sum accuracy.

GCMC sampling was performed using a Metropolis Monte Carlo scheme with three types of moves: exchange (consisting of creation and deletion of a CH_4 molecule), translation, and rotation, with respective probabilities of 2:1:1. Uptake at each fugacity was evaluated by first equilibrating for 10^6 steps, followed by 2 × 10^6 production steps. Isotherms were calculated for a fugacity range of 0−100 bar corresponding to pressures of 0−120 bar at 298 K. The excess adsorption is computed according to $N_{excess} = N - \rho_{bulk}V_{pore}$, where N is the total number of adsorbed molecules, ρ_{bulk} is the bulk density of methane at a specified temperature and pressure, and V_{pore} is the pore volume of the MOF which was calculated using the PLATON[59] code.

To quantify the accuracy of the GCMC predictions, and their sensitivity to the choice of interatomic potential, isotherms were calculated using several existing potential forms and compared against experimental data.[18,21,22,27] Four descriptions of the CH_4 molecule were considered:

1. TraPPE:[48] represents methane as a neutral, single-site spherical molecule
2. Five-site model:[50] a charged five-site model where C and H atoms are assigned charges of −0.66 and 0.165, respectively
3. AA (all atom) model:[51] a neutral five-site model
4. TraPPE-EH:[49] an uncharged extension of the TraPPE model in which fictitious H atom sites are added at the center of the four C−H bonds

Two parametrizations were examined for atoms associated with the MOF: (i) UFF,[52] the universal force field, is used for all MOF atoms, and (ii) DREIDING[53] parameters are used for

dx.doi.org/10.1021/jp4104273 | J. Phys. Chem. C 2014, 118, 2929−2942

H, C, and O atoms, with UFF[52] parameters for the metal sites. To simplify notation, we adopt the abbreviations "U" for UFF-based potentials and "D-U" for the potential that mixes parameters from DREIDING and UFF.

Combining the description of the CH_4 molecule with the two descriptions for the MOF, a total of six sets of force fields were considered: (i) D-U+Five-site, (ii) D-U+TraPPE, (iii) U +Five-site, (iv) U+TraPPE, (v) D-U+AA, and (vi) D-U +TraPPE-EH. These models were compared against experimental data for CH_4 adsorption in M-DOBDC with M = Mg, Mn, Co, Ni, and Zn.[22] The D-U+TraPPE potential was found to best reproduce the measured uptake data. This model was subsequently applied to the remainder of the M-DOBDC series and to MOF-5, PCN-11, PCN-14, and HKUST-1.

3. RESULTS AND DISCUSSION

DFT Benchmarking. Calculations on an alkaline earth and a transition metal based system—Mg- and Ni-DOBDC—were used to assess the accuracy of several "conventional" (i.e., PBE-GGA) and dispersion-corrected density functionals with respect to experimental adsorption enthalpies. These included the semiempirical DFT-D2[38] and the vdW-DF method with five distinct exchange functionals: revPBE (vdW-DF1),[39] optB86b,[60] optB88,[61] optPBE,[61] and rPW86 (vdW-DF2).[41] Figure 1 and Table S2 in the Supporting Information compare

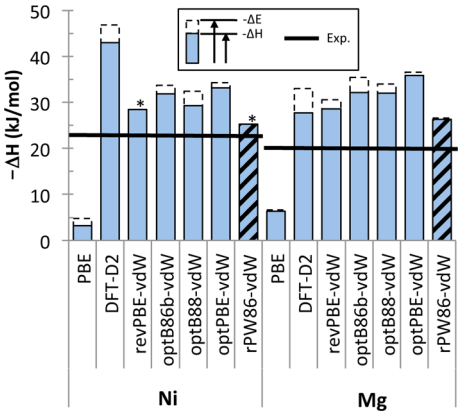

Figure 1. Comparison of calculated CH_4 adsorption energies in Mg and Ni-DOBDC as a function of calculation method with experimental data (ref 22). Adsorption enthalpies (ΔH) at 300 K are represented by solid columns. Cross-hatching is used to highlight the vdW-DF2 method (rPW86-vdW), which yields the best agreement with experimental data. The total column height corresponds to the 0 K static binding energy (ΔE); the dashed portion indicates the sum of zero point (ZPE) and thermal energy (TE) contributions. The experimental CH_4 adsorption enthalpy is depicted using a horizontal line. An asterisk indicates cases where ZPE + TE contributions are negative; see Table S2 in the Supporting Information for numerical data.

the calculated ΔH values for Mg- and Ni-DOBDC with the experimental enthalpies from ref 22. The experimental data were extrapolated to a coverage of 1 CH_4 per metal site by adding 2.7 kJ/mol to the reported enthalpies. The dashed portions of the columns in Figure 1 represent the summed contribution of zero point (ΔE_{ZPE}) and thermal (ΔE_{TE}) energies to ΔH at 300 K. This contribution is typically endothermic,[34,43] ranging from 0.3 to 5.4 kJ/mol. [Exceptions occur for Ni-DOBDC in the cases of the revPBE (vdW-DF1) (−0.1 kJ/mol) and vdW-DF2 (−1.4 kJ/mol) functionals.]

As shown in Figure 1, the PBE-GGA significantly underpredicts the experimental ΔH in both MOFs, with an average absolute error of 18 kJ/mol. The use of dispersion corrections greatly improves agreement with the experimental enthalpies, although in all cases the calculated ΔH values somewhat overestimate experiments. The best agreement is obtained with the vdW-DF2 functional, which uses rPW86-based exchange. In this case the calculated ΔH for Mg- and Ni-DOBDC are, respectively, −26.3 and −25.3 kJ/mol. Sillar et al.[62] reported a methane adsorption enthalpy of −26.4 kJ/mol on Mg-DOBDC using a hybrid method based on MP2/PBE+D, in good agreement with our value. Compared to experiments, vdW-DF2 exhibits a small MAD of 3.7 kJ/mol, which is followed by the vdW-DF1 method (revPBE-based exchange) with an error of 6.4 kJ/mol. Comparable accuracy was reported for these two functionals in the case of CO_2 adsorption in MOFs.[34,43] MAD values for the other dispersion-corrected functionals range from 9 to 13 kJ/mol. Given that the rPW86 and revPBE based vdW-DFs most closely reproduce the experimental enthalpies, we have adopted these functionals for calculations on the remaining M-DOBDC variants.

Thermodynamic Properties. Table 2 summarizes the methane adsorption enthalpies computed with the vdW-DF2 method across all 18 metal-substituted DOBDC variants; experimental data for Mg-, Mn-, Co-, Ni-, and Zn-DOBDC from refs 22 and 57 is included for comparison. These same data are depicted graphically in Figure 2. Contributions from

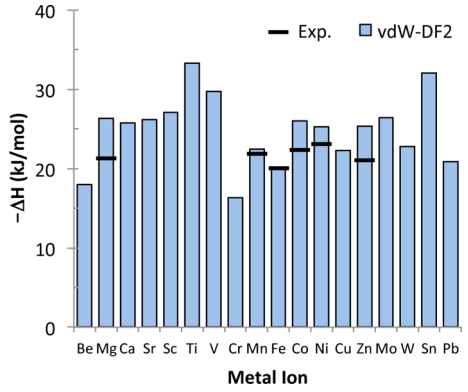

Figure 2. Adsorption enthalpies (ΔH) at T = 300 K for 18 metal-substituted DOBDC MOFs calculated using the vdW-DF2 functional. Black horizontal lines indicate the experimental enthalpies from refs 22 and 57.

Table 2. Calculated Adsorption Enthalpies (kJ/mol CH_4) from vdW-DF2 for 18 Metal-Substituted Variants of M-DOBDC[a]

	Be	Mg	Ca	Sr	Sc	Ti	V	Cr	Mn	Fe	Co	Ni	Cu	Zn	Mo	W	Sn	Pb
calcd	18.1	26.3	25.8	26.2	27.1	33.3	29.7	16.4	22.5	19.9	26	25.3	22.3	25.4	26.4	22.8	32	20.9
expt		21.2							21.8		22.3	22.9		21				

[a]Experimental data are taken from refs 22 and 57.

dx.doi.org/10.1021/jp4104273 | J. Phys. Chem. C 2014, 118, 2929−2942

the static binding energy (ΔE), zero point energy (ΔE_{ZPE}), and thermal energy (ΔE_{TE}) to the CH_4 adsorption enthalpies are given for vdW-DF2, vdW-DF1, and the PBE-GGA in Table S3 in the Supporting Information. Consistent with the preceding benchmarks, the vdW-DF2 method most accurately reproduces the experimental ΔH across the five M-DOBDC variants for which measurements have been reported. For this method the MAD of 2.7 kJ/mol is slightly less than that for vdW-DF1, 3.8 kJ/mol. In further agreement with experiments, the calculated ΔH values across these five M-DOBDC systems are relatively constant, varying by only 3−4 kJ/mol.

Across the full range of metal substitutions the methane adsorption enthalpy (ΔE) varies from −16.4 kJ/mol in the least exothermic case of Cr-DOBDC to −33.3 kJ/mol in Ti-DOBDC, which has the most exothermic interaction with CH_4 overall. In addition to Cr, the other M-DOBDC variants that bind CH_4 relatively weakly ($|\Delta H| < 23$ kJ/mol) include Be, Fe, Pb, Cu, Mn, and W. At the opposite extreme, Sn and V (in addition to Ti) show the strongest affinities for methane with $\Delta H = -32$ and −29.7 kJ/mol, respectively. Ni, Zn, Ca, Co, Sr, Mg, Mo, and Sc fall in the intermediate ΔH range of −25 to −27 kJ/mol.

To put these values into perspective, earlier calculations[34] of adsorption enthalpies for CO_2 on M-DOBDC reported interactions which were much more exothermic and which exhibited a wider range of values: $\Delta H = -25$ to −53.5 kJ/mol at 300 K. Clearly CH_4 adsorption in M-DOBDC is generally weaker than for CO_2. Nevertheless, several trends are shared between these two adsorbates. For example, adsorption in the 3d metals is strongest for the early transition metals (Sc, Ti, V). Moving to the right in the periodic table, the interaction weakens for Cr and then roughly strengthens again as one continues across the 3d series. The trends between CO_2 and CH_4 are also similar for the alkaline and alkaline earth metals, where Mg, Ca, and Sr exhibit relatively strong adsorptive interactions with both molecules. A shared exception is the lower binding energy for Be-DOBDC. Upon relaxation, Be becomes buried (and therefore inaccessible) inside the MOF structure, preventing direct interactions with the adsorbed guest molecule, and resulting in less exothermic adsorption enthalpies. Consequently, a site slightly displaced toward the ligand is the preferred location for CO_2 adsorption in Be-DOBDC.[34]

Electronic Structure. The different magnitudes of the adsorption enthalpies for CO_2 versus CH_4 on M-DOBDC can be attributed to differences in the strength of electrostatic interactions between the CUS and the adsorbate molecules. Although neither CO_2 nor CH_4 possesses a permanent dipole, they differ in their polarizability and distribution of atomic charges. CO_2 is more polarizable, and its outer oxygen atoms have a net negative charge. These two factors result in a more exothermic interaction with (positive) CUS ions, and a more pronounced sensitivity to the charge state of the metal, which is manifested as a wider range in ΔH.[34] In contrast, CH_4 has a lower polarizability and its hydrogen atoms have a slightly positive charge, resulting in less exothermic, and more uniform, interactions with the CUS.

Evidence that electrostatic interactions play a smaller role in CH_4 adsorption can be seen in the charge density difference plots of Figure 3, which compare the degree of charge redistribution upon adsorption of CH_4 and CO_2 on Mg-DOBDC. (Additional data for M = Sn, Mo, and Zn are presented in Figure S1 in the Supporting Information.)

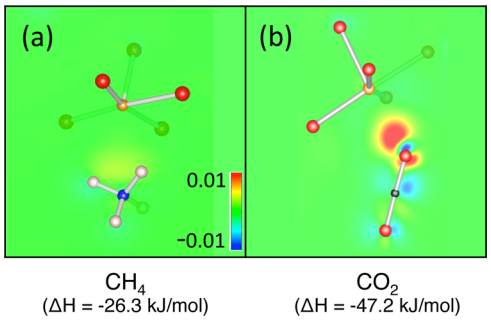

Figure 3. Charge density difference plots (relative to the isolated components) for (a) CH_4 and (b) CO_2 adsorption (ref 34) on Mg-DOBDC. For simplicity, only the CUS metal and its nearest neighbors are shown. Red represents charge accumulation and blue is charge depletion. Blue spheres = C, white = H, gold = Mg, and red = O.

Compared to CO_2,[34] the degree of charge density redistribution on CH_4 and in the regions between CH_4 and the MOF is much smaller (0.011 e/Å^3 for CO_2 vs 0.003 e/Å^3 for CH_4), consistent with the smaller CH_4 adsorption enthalpy (~21 kJ/mol less exothermic than for CO_2), and suggesting that van der Waals interactions play a more dominant role in CH_4−MOF adsorption. The charge density redistribution for CO_2 in Mg-DOBDC has a maximum that is 20% greater than for CH_4 in Mo-DOBDC (Supporting Information, Figure S1b), and also occurs over a larger region. Although there is no significant charge redistribution between CUS and CH_4 in Sn-DOBDC (Supporting Information, Figure S1d), however, the somewhat more exothermic adsorption enthalpy (as described below) originates from secondary interactions involving the ligand.

Local density of states (LDOS) plots for Mg-, Mo-, Zn-, and Sn-DOBDC before and after CH_4 adsorption are shown in Figure S1 in the Supporting Information. Although there is no noticeable change in the MOF metal-projected DOS upon adsorption, in all cases the CH_4 states shift toward lower energies, consistent with the presence of a weak electrostatic component to binding. A larger shift in the CO_2 DOS upon adsorption was previously observed in these systems.[34] Additional evidence that van der Waals contributions are the primary component of the CH_4 binding energy is given in Table S4 in the Supporting Information, which shows that the van der Waals contribution is generally large and exothermic. Finally, we recall that adsorption of CO_2 in M-DOBDC and M-HKUST-1 was accompanied by a large distortion in the CO_2 molecular geometry.[34,43] However, no significant change of this type is observed in the case of CH_4.

Our prior study of CO_2 capture in metal-substituted MOFs identified a trend relating the magnitude of ΔH to the effective charge on the CUS.[34] This trend arose from the strong electrostatic contributions to the CO_2−MOF interaction. In the case of CH_4 adsorption, Table S4 and Figure S3c in the Supporting Information show (with the exception of Sn) the presence of a similar, but somewhat weaker, trend. That this trend is less pronounced for CH_4 is consistent with the smaller role played by electrostatics in this system. [Due to its unique adsorption geometry (as discussed previously), these correlations often do not hold for Sn-DOBDC.] In addition, Figure S3b in the Supporting Information shows that ΔH weakly correlates with the ionic radius of the CUS, in cases where the radius is relatively small (<1.0 Å). This trend can be explained as follows: In the adsorbed MOF complexes, hydrogen from CH_4 is in close proximity to the carboxyl oxygen atoms on the

dx.doi.org/10.1021/jp4104273 | J. Phys. Chem. C 2014, 118, 2929−2942

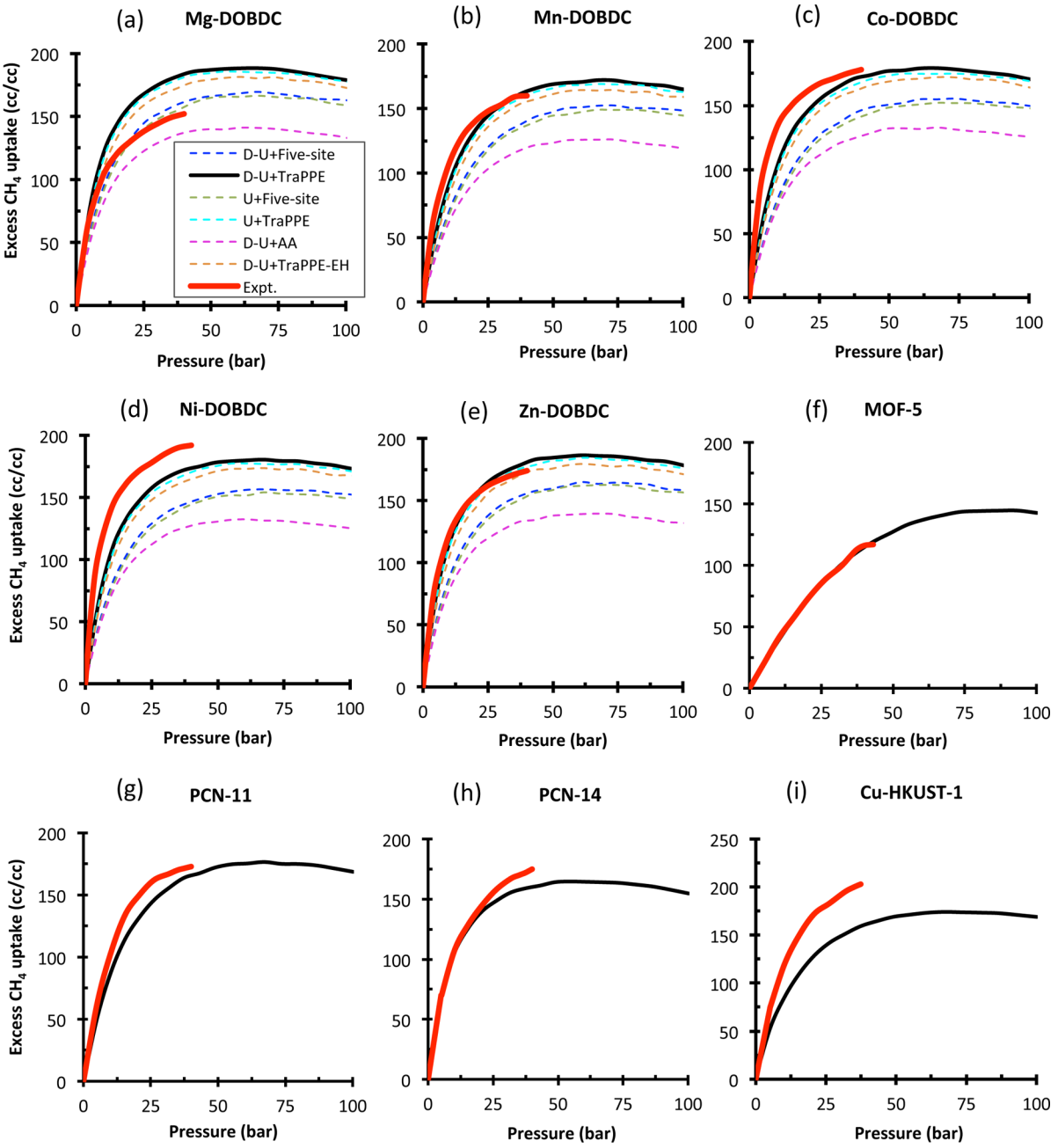

Figure 4. Comparison of calculated excess CH_4 adsorption isotherms (at 298 K) evaluated using six distinct force fields with experimental isotherms for [Mg, Mn, Co, Ni, Zn]-DOBDC, MOF-5, and PCN-11 and for PCN-14 and Cu-HKUST-1 (refs 18, 21−23, and 24). Descriptions of the force-field models are provided under Methods. Experimental isotherms are depicted using a solid red line; the black solid line highlights the performance of the D-U+TraPPE force field, which yields the best overall agreement with the experimental data.

MOF, while the carbon from CH_4 approaches the MOF's CUS. Such an arrangement minimizes the separation between pairs of oppositely charged (attracting) atoms. An increase to the ionic radius of the CUS elongates metal−O bonds in the MOF and allows the bulky CH_4 to approach the framework more closely. This has the effect of minimizing these bond lengths and increasing the strength of interaction. Finally, Table S5 and Figure S3d in the Supporting Information illustrate a clear trend between increasing bond exothermicity (more negative ΔH) and decreasing metal−C(CH_4) and O−H(CH_4) distances.

Experiments[22] have demonstrated that CUS are the primary adsorption site for CH_4 in DOBDC at pressures up to a loading of 1 CH_4 per metal. At higher loadings other sites will become occupied; however, these secondary (or tertiary) sites have not been widely explored. To probe these, calculations were performed at several alternative adsorption sites in Ni-DOBDC. The three sites identified as being most energetically favorable are illustrated in Figure S2 in the Supporting Information. We find that the adsorption energy at the carboxyl oxygen site (Supporting Information, Figure S2b) adjacent to the CUS is comparable to that at the CUS: the carboxyl site is only 0.3 kJ/mol less favorable (ΔE = −23.6 kJ/mol) than the CUS site (Supporting Information, Figure S2a, ΔE = −23.9 kJ/mol), likely due to the fact that CH_4 maintains a similar bond length (3.54 Å) to the CUS in this position.

dx.doi.org/10.1021/jp4104273 | J. Phys. Chem. C 2014, 118, 2929−2942

Binding to the aromatic ring C-site (Supporting Information, Figure S2c) is somewhat weaker: ΔE = −20.6 kJ/mol. Calculated bond distances between C (in CH_4) and the different MOF sites correlate with the binding energy: 3.29 (metal site), 3.53 (carboxyl O-site), and 3.70 Å (C-ring site).

Comparison of Interatomic Potentials. The methane storage capacity predicted by GCMC calculations will depend upon the interatomic potentials used to describe the interaction between methane and the MOF. It is therefore helpful to examine the degree to which common potentials reproduce experimental isotherms.[25,31,40,63,64] Here we explore how varying the force-field properties—e.g., presence/absence of partial atomic charges, unified atom versus a five-site model of CH_4, etc.—impacts the accuracy of the predicted storage capacity. The performance of six distinct force fields is assessed (details are provided under Methods): D-U+Five-site, D-U +TraPPE, U+Five-site, U+TraPPE, D-U+AA, and D-U +TraPPE-EH. Comparisons are made first to the experimental excess adsorption isotherms reported by refs 22 and 24 across a series of five M-DOBDC compounds with M = Mg, Mn, Co, Ni, and Zn, and are subsequently extended to MOF-5, HKUST-1, PCN-11, and PCN-14.[18,21,24]

Figure 4a–e compares the methane isotherms for M-DOBDC calculated with these force fields to experimental measurements.[22,24] Several observations can be made from these data. First, varying the LJ parameters of the MOF atoms between the UFF (U) and Dreiding+UFF (D-U) force fields results in a negligible difference in the predicted isotherms. This is not surprising given that both models use LJ parameters from the UFF to describe the CUS, and the CUS site is the primary adsorption site (Supporting Information, Figure S4). Second, the predicted uptake is much more sensitive to the potential used to describe the methane molecule. For example, the uncharged all atom (AA) model for CH_4 shows the greatest deviation with experiments, and consistently (and significantly) underestimates the measured uptake. Likewise, methane uptake is generally underpredicted by the five-site charged model. Overall, we find that the D-U+TraPPE model (solid black line) yields the best agreement with experiments. As the TraPPE-EH potential is closely related to the TraPPE, we expect (and observe) that isotherms predicted by these two force fields are similar.

The performance of the six force fields in reproducing the experimental CH_4 uptake for M-DOBDC has been quantified by evaluating the mean absolute deviation (MAD). The MAD was calculated as an average over the deviation in CH_4 uptake at eight pressures in the range 0.1–35 bar: 0.1, 5, 10, 15, 20, 25, 30, and 35 bar. Comparisons at lower pressures such as 5 bar are desirable because estimates of usable capacity rely on the differential uptake at 5 bar and at higher pressures. The MAD for each force field averaged across the M-DOBDC series is summarized in Figure 5a. Deviations are smallest (16 cm^3/cm^3) for the D-U+TraPPE model and largest (45 cm^3/cm^3) for the uncharged all atom (AA) potential.

The performance of the D-U+TraPPE force field was examined further by comparing its predicted CH_4 uptake to experimental data for four other prominent MOFs: MOF-5,[18] PCN-11,[21] PCN-14,[24] and HKUST-1.[24] Calculated excess isotherms are shown in Figure 4f–i, while Figure 5b plots the MAD for each individual compound. The simulated isotherms are in reasonably good agreement with measurements, especially for the cases of MOF-5, PCN-11, and PCN-14. In these three MOFs the MAD with respect to experimental

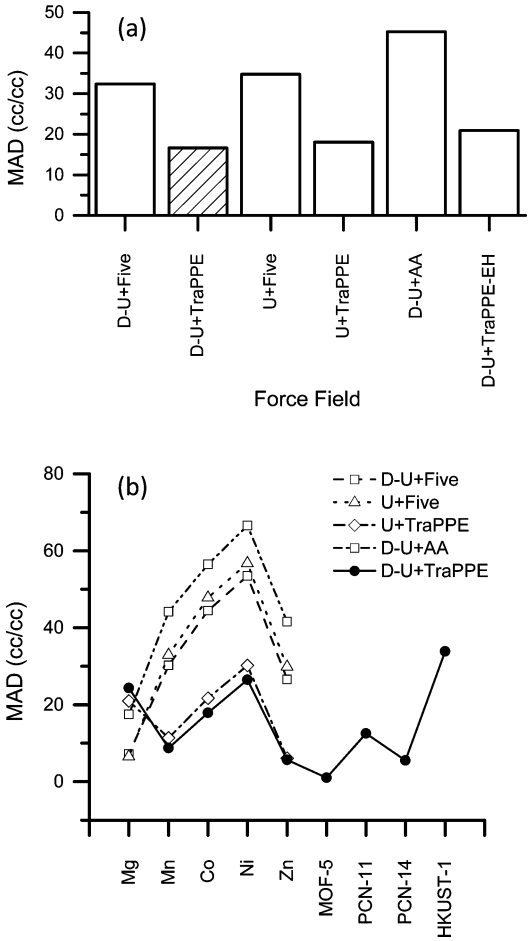

Figure 5. Mean absolute deviation (MAD) between the calculated CH_4 uptake and experiments. (a) MAD as a function of interatomic potential. Here the MAD is averaged over five M-DOBDC variants (M = Mg, Mn, Co, Ni, Zn). The best-performing potential, D-U+TraPPE, is highlighted with cross-hatching. (b) MAD for individual MOFs.

uptake ranges from a low of 1.0 cm^3/cm^3 (MOF-5) to a high of 12.5 cm^3/cm^3 (PCN-11) for the pressure range 0.1–35 bar. However, the agreement with experiments is somewhat worse for HKUST-1 (MAD = 33), with GCMC underpredicting CH_4 uptake, similar to what has been observed in prior studies.[65] Likewise, inspection of the isotherms for PCN-11 and PCN-14 (Figure 4g,h) also shows that GCMC systematically underestimates uptake in these MOFs, albeit to a smaller degree. In all three of these MOFs the deviation from experiments is small at low CH_4 loading (i.e., low pressures), but then grows as the loading increases. Notably, the tendency for GCMC to underpredict uptake does not apply to the M-DOBDC compounds, which also contain CUS.

These trends can be understood by referring to previous experiments[22,30,65] and GCMC modeling.[30,65] In the cases of PCN-11, PCN-14, and HKSUST-1, it is known[30,65] that conventional classical potentials do not properly account for interactions with the Cu CUS, resulting in limited adsorption at these sites. (Our calculations confirm this behavior—see Figure S4 in the Supporting Information for a plot of the methane adsorption density in PCN-11, PCN-14, and HKUST-1.) Nevertheless, diffraction experiments[30,65] have shown that these same sites are primary sites for CH_4 adsorption, with a high occupancy (93%)[65] of CH_4 under saturation conditions. In the regime of low loadings/low pressures, it has been reported

dx.doi.org/10.1021/jp4104273 | J. Phys. Chem. C 2014, 118, 2929–2942

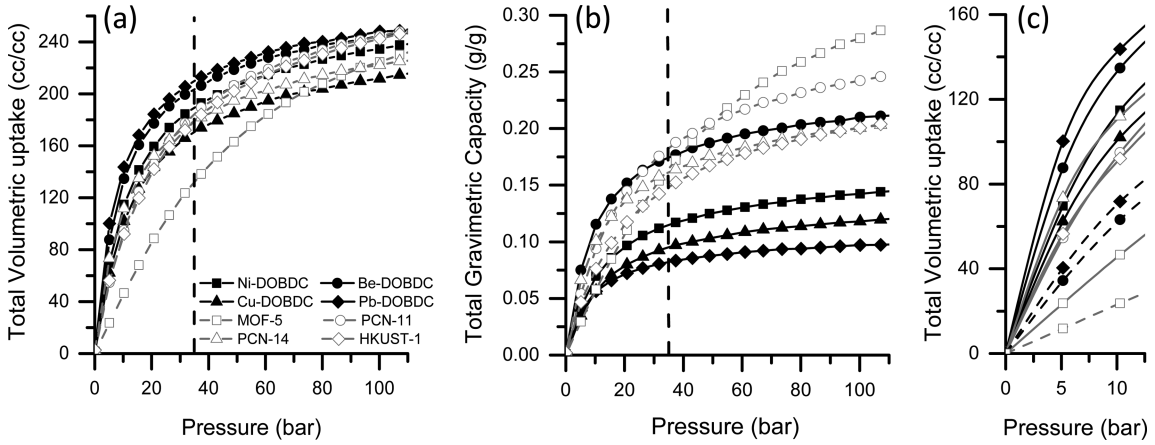

Figure 6. Calculated CH_4 adsorption isotherms (evaluated using the D-U+TraPPE interatomic potential) for selected M-DOBDC variants, and for MOF-5, PCN-11, PCN-14, and HKUST-1. (a) Total volumetric uptake (cm^3/cm^3) for 0−100 bar and 298 K. The vertical dashed line indicates a pressure of 35 bar, which is the pressure at which the DOE storage targets are specified. (b) Total gravimetric uptake (g/g) for 0−100 bar and 298 K. (c) Magnification of the volumetric isotherms in (a) at low pressure, P = 0−12.5 bar. Dashed isotherms are for T = 358 K.

Table 3. Predicted Volumetric (cm^3/cm^3) and Gravimetric (g/g) CH_4 Storage Capacities in Several MOFs as a Function of Pressure and Temperature[a]

	P_{max} = 35 bar				P_{max} = 65 bar				P_{max} = 100 bar			
	total		usable		total		usable		total		usable	
	298 K		298 K (PS)	358 K (TPS)	298 K		298 K (PS)	358 K (TPS)	298 K		298 K (PS)	358 K (TPS)
MOF	cm^3/cm^3	g/g	cm^3/cm^3	cm^3/cm^3	cm^3/cm^3	g/g	cm^3/cm^3	cm^3/cm^3	cm^3/cm^3	g/g	cm^3/cm^3	cm^3/cm^3
Be-DOBDC	204	0.17	118	169	230	0.20	144	195	245	0.21	160	211
Mg-DOBDC	200	0.16	122	168	228	0.18	150	196	243	0.20	165	211
Ca-DOBDC	187	0.15	123	161	218	0.18	153	191	235	0.19	170	208
Sr-DOBDC	175	0.11	116	150	206	0.13	147	181	222	0.14	163	197
Sc-DOBDC	179	0.11	100	147	198	0.12	119	166	211	0.13	132	179
Ti-DOBDC	192	0.13	128	165	223	0.16	159	196	240	0.17	176	213
V-DOBDC	189	0.12	124	162	220	0.15	155	193	237	0.16	171	210
Cr-DOBDC	178	0.11	117	152	207	0.13	147	182	225	0.14	164	199
Mn-DOBDC	178	0.12	123	155	210	0.14	155	187	228	0.15	173	205
Fe-DOBDC	185	0.12	127	160	215	0.14	157	190	233	0.15	175	208
Co-DOBDC	188	0.12	124	162	218	0.14	154	191	234	0.15	170	208
Ni-DOBDC	189	0.11	122	162	217	0.13	150	189	234	0.14	167	207
Cu-DOBDC	171	0.10	111	145	197	0.11	137	172	212	0.12	152	187
Zn-DOBDC	196	0.12	121	166	225	0.14	150	195	241	0.15	166	210
Mo-DOBDC	174	0.08	115	149	200	0.10	141	175	215	0.10	156	190
W-DOBDC	183	0.06	118	156	210	0.07	145	183	226	0.08	160	198
Sn-DOBDC	197	0.09	98	157	219	0.10	120	179	234	0.11	135	194
Pb-DOBDC	210	0.08	113	169	234	0.09	138	194	248	0.10	152	208
MOF-5	132	0.16	110	120	189	0.24	168	178	225	0.28	203	213
PCN-11	183	0.18	130	159	222	0.22	169	198	244	0.24	191	220
PCN-14	178	0.16	108	148	205	0.19	134	175	222	0.20	151	192
HKUST-1	178	0.15	125	152	219	0.18	165	192	242	0.20	188	215

[a]All capacities include adsorbed and gas-phase CH_4. "Total" refers to the capacity at 298 K assuming an isothermal pressure swing between the maximum pressure (P_{max} = 35, 65, or 100 bar) and 0 bar. "Usable" refers to the capacity obtained from either an (a) isothermal (298 K) pressure swing (PS) between P_{max} and 5 bar or (b) temperature + pressure swing (TPS) from 298 K and P_{max} to 358 K and 5 bar. Volumetric capacities are calculated assuming a single-crystal MOF monolith; in a practical storage system the volumetric density will be lower due to losses arising from inefficient packing of the (polycrystalline) MOF media.

that the CUS fill more slowly than the more easily accessed "pocket" sites: for example, in HKUST-1 only 44% of the CUS are occupied at 59% of maximum loading.[65] On the other hand, adsorption within the pocket sites is correctly captured by GCMC.[30,31] Taken together, these observations suggest that the omission of enhanced CH_4−CUS binding in classical potentials will result in an underprediction of CH_4 uptake that is small at low coverage, but then grows as the CH_4 loading increases. This same trend is observed in Figure 4g−i. We also expect that the extent to which GCMC underestimates experiments will correlate with the fraction of CH_4 molecules adsorbed at CUS. At 35 bar and 298 K, experiments find the fraction of adsorbed CH_4 at CUS to be largest in HKUST-1 (61%) and somewhat smaller in PCN-11 (41%) and PCN-14

dx.doi.org/10.1021/jp4104273 | J. Phys. Chem. C 2014, 118, 2929−2942

(27%).[30] These percentages track the MAD for these three compounds (Figure 5b).

In contrast to the behavior of HKUST-1, PCN-11, and PCN-14, GCMC calculations on the M-DOBDC series show no such systematic deviation with the experimental uptake. This is because GCMC *does* correctly reproduce the CUS as being the primary CH_4 adsorption site[22] (see the CH_4 density distribution plots for Mg- and Ni-DOBDC in the Supporting Information, Figure S4.) The reason that the CUS sites are property treated in M-DOBDC with classical potentials may be due to the fact that in M-DOBDC the CUS sites coincide with corner sites in the framework, where enhanced vdW interactions are likely to occur.

To test this hypothesis, we calculated the CH_4 uptake in a fictitious MOF, "C-DOBDC," in which the Ni CUS from Ni-DOBDC was replaced with a C atom. Figure S10 in the Supporting Information compares the CH_4 density distribution for Ni-DOBDC and C-DOBDC, revealing that there is no significant difference between these MOFs. Moreover, the calculated CH_4 uptake in both cases differs by less than 10% (~15 cm^3/cm^3). Finally, the isosteric heats of adsorption, Q_{st}, calculated using the classical potentials (Supporting Information, Table S8) show almost no sensitivity to the composition of the CUS, unlike the DFT or experimental data (Table 2). These calculations confirm that it is the geometry of the corner-like CUS site, rather than the presence of the CUS itself, which makes these sites preferred locations for CH_4 adsorption in DOBDC.

Despite these limitations, the simple D-U+TraPPE potential yields quite reasonable predictions of CH_4 capacity: including data from all nine MOFs, we find that the D-U+TraPPE force field exhibits a MAD of 15 cm^3/cm^3 across the range of 0.1−35 bar. (For comparison, evaluating the MAD at a single pressure of 35 bar gives a MAD of 14 cm^3/cm^3.) As most high-capacity MOFs have excess CH_4 capacities exceeding 150 cm^3/cm^3, a MAD of this magnitude would result in an error of approximately 10%. While we believe this is sufficient to enable screening of candidate MOFs,[25] outliers with larger deviations on the order of 30 cm^3/cm^3 (such as HKUST-1) do exist (Figure 4i). Hence, further optimization of CH_4−MOF force fields would be welcome.[31]

Of course one should not forget that variation in the synthesis and measurement of CH_4 uptake may also contribute to the deviations observed with simulation. For example, follow-up measurements[24] of methane adsorption on Ni-DOBDC and PCN-14 found that total uptake capacity at 35 bar differed from previous reports[22,27] by 28−35 cm^3/cm^3; similar differences were observed for HKUST-1.[24,66,67] To address these uncertainties, round-robin testing by different groups on a small number of prototype materials would clearly be beneficial. With these caveats in mind, we have employed the D-U+TraPPE force field to predict total methane storage capacities across the remainder of the M-DOBDC series, and to examine the effect of realistic operating conditions on the achievable (i.e., usable) CH_4 capacity.

CH_4 Storage Capacity. The methane storage capacity was evaluated for pressures up to 100 bar, and was tabulated for three operating scenarios using maximum working pressures, P_{max}, of 35, 65, and 100 bar. The operating scenarios include the following: (i) *total capacity* at 298 K and P_{max}; (ii) *usable capacity* at 298 K, assuming an isothermal pressure swing (PS) from P_{max} to 5 bar; (iii) *usable capacity* assuming both a temperature and pressure swing (TPS) from 298 K and P_{max} to 358 K (85 °C) and 5 bar. Total methane uptake isotherms at 298 K for P = 0−100 bar are shown in Figure 6 for four representative MOFs from the M-DOBDC series (M = Ni, Cu, Be, and Pb) and for MOF-5, PCN-11, PCN-14, and HKUST-1. A summary of the storage capacities for all 22 MOFs across all operating scenarios is given in Table 3; isotherms for all compounds are provided in Figure S5 in the Supporting Information. In the following sections we first report total capacities, and then subsequently expand our analysis to consider usable capacities under PS and TPS operating scenarios.

Total Capacity. We define the total methane capacity at a specified temperature (298 K) and pressure P_{max} as the sum of CH_4 stored in a single-crystal MOF monolith both as adsorbed molecules on the surfaces of pores and as gas-phase molecules within those pores. The total capacity is an upper bound to the achievable (or usable) capacity in a practical storage system, given the following:

(i) The total capacity represents the capacity that could hypothetically be achieved if *all* CH_4 could be removed from the MOF. For PS operation, this would require a vanishing pressure of CH_4 within the storage vessel, whereas the DOE targets (Table 1) specify a lower pressure limit of 5 bar.

(ii) The adsorbent media in a practical system will exhibit a lower packing density than that of a hypothetical single-crystal monolith. Consequently, a viable CH_4 storage material must have a total capacity that (likely far) exceeds the targets.

Figures 6a and 7 illustrate that, for P_{max} = 35 bar, the total volumetric capacities of the MOFs studied here fall within the range 171−210 cm^3/cm^3. (MOF-5 is an exception to this trend, with a much lower capacity of 132 cm^3/cm^3.) In the case of the M-DOBDC compounds, the comparable volumetric capacities can be explained by the fact that the CUS act as primary adsorption sites,[22] and the density of these sites is similar across the nominally isostructural M-DOBDC series, ranging from 3.62 to 4.98 sites/nm^3 (Supporting Information, Table S6). Two hypothetical M-DOBDC compounds with M = Be and Pb are predicted to have the highest total volumetric uptake at 204 and 210 cm^3/cm^3, respectively. Moreover, several other

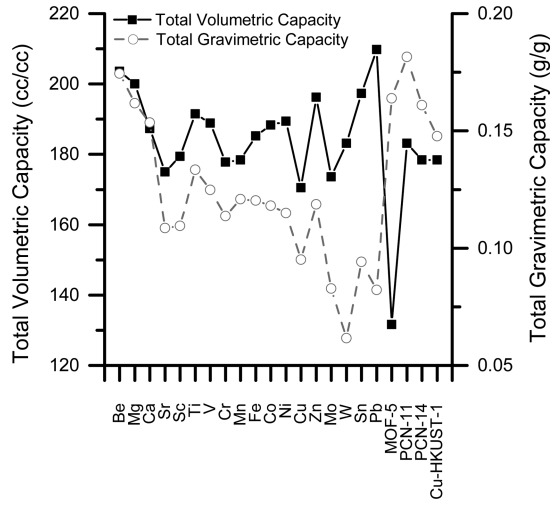

Figure 7. Total CH_4 uptake at 35 bar and 298 K on a volumetric (left axis) and gravimetric (right axis) basis. Calculations were performed using the D-U+TraPPE force field; metal symbols (M) along the *x*-axis refer to the composition of M-DOBDC.

dx.doi.org/10.1021/jp4104273 | J. Phys. Chem. C 2014, 118, 2929−2942

members of the M-DOBDC family (M = Mg, Ca, Ti, V, Fe, Co, Ni, Zn, W, and Sn) have calculated total capacities exceeding 180 cm^3/cm^3 (Table 1). Similar volumetric capacities of 178−183 cm^3/cm^3 are predicted for PCN-11, PCN-14, and HKUST-1.

Unfortunately, the volumetric benefits conferred by the high density of CUS in the M-DOBDC compounds generally come at a cost to gravimetric performance. Figures 6b and 7 illustrate this trade-off. For example, even though Pb-DOBDC has the highest total volumetric capacity at P_{max} = 35 bar, the high mass of Pb (207.2 amu) results in this compound having the second-lowest gravimetric uptake overall (0.08 g/g). Conversely, M-DOBDC compounds in which the CUS consist of the light alkaline earth metals Be and Mg have among the best gravimetric capacities, 0.17 and 0.16 g/g, respectively. Given that these compounds also have high volumetric capacities (204 and 200 cm^3/cm^3, Table 3), this pair of MOFs exhibits the best combination of total volumetric and gravimetric CH_4 capacity under these conditions. Continuing the correlation of gravimetric capacity with the mass of the CUS, M-DOBDC compounds for which M consists of a first row transition metal have somewhat lower capacities of 0.10−0.13 g/g. Finally, gravimetric capacities are also high in PCN-11, PCN-14, and HKUST-1, ranging from 0.15 to 0.18 g/g. Although these compounds have Cu-based CUS, the density of these sites is lower than in the M-DOBDC series (1.82−2.58 sites/nm^3), lessening their gravimetric penalty.

If operation at pressures above 35 bar is possible, then slightly higher total capacities can be achieved. Figure 6a,b illustrates CH_4 uptake isotherms for selected MOFs for pressures up to 100 bar, while Table 2 summarizes total capacities at P_{max} = 65 and 100 bar. For the best-performing MOFs at 35 bar, Be- and Mg-DOBDC, a near doubling of P_{max} to 65 bar results in only a small 13% increase in volumetric capacity (228−230 cm^3/cm^3) and a 15% increase in gravimetric capacity (0.18−0.20 g/g). At these pressures the capacity of PCN-11 (222 cm^3/cm^3, 0.22 g/g) also begins to "catch up" with these two compounds. Increasing the pressure further to 100 bar results in diminishing capacity gains in all three of these compounds of only 7−9% for both volumetric and gravimetric CH_4 densities. At this pressure PCN-11 attains the best overall capacity of 244 cm^3/cm^3 and 0.24 g/g, while Be/Mg-DOBDC and HKUST-1 are close runners up (242−245 cm^3/cm^3 and 0.20−0.21 g/g). Although these high total capacities represent a best-case scenario, they are only 70% of the DOE volumetric target of 349 cm^3/cm^3, and less than half (48%) of the 0.5 g/g gravimetric target (Table 1). As we describe next, accounting for residual CH_4 present at the lower pressure limit of 5 bar (i.e., during a pressure swing) further reduces these capacities.

Usable Capacity: Isothermal Pressure Swing (PS). As previously described, the usable capacity differs from the total capacity in that the former assumes a minimum operating pressure of 5 bar (consistent with the DOE targets), while the latter assumes the hypothetical desorption of all CH_4, corresponding to a minimum pressure of 0 bar. Figure 6c magnifies the adsorption isotherm for selected MOFs from Figure 6a within the low-pressure region, P < 12.5 bar. With the exception of MOF-5, it is clear that each of the examined MOFs retains significant quantities of CH_4 at 5 bar. These "residual capacities" range from 53 cm^3/cm^3 in HKUST-1 and PCN-11 to 97 cm^3/cm^3 in Pb-DOBDC, and represent 30−46% of the total volumetric capacity at 35 bar. In contrast, the CH_4 capacity of MOF-5 at 5 bar is only 22 cm^3/cm^3. The smaller uptake in MOF-5 can be attributed to the absence of EBS in its crystal structure. In contrast, all of the other MOFs examined here contain EBS. The increased interactions occurring at EBS—be they through enhanced electrostatics at CUS or enhanced vdW bonding at pocket sites—results in a more rapid filling of these sites at low pressures, which is manifested as a steeper rise in the isotherms of these MOFs.[65]

The consequences of significant residual CH_4 capacity at low pressure can be seen in Table 3. The calculated usable volumetric capacities assuming a PS to 5 bar are significantly lower than the *total* capacities. (Usable gravimetric capacities are reported in Table S7 in the Supporting Information.) For P_{max} = 35 bar, PCN-11 exhibits the highest usable volumetric capacity of 130 cm^3/cm^3 and the second highest gravimetric capacity of 0.13 g/g. These values are 28−38% smaller than the largest *total* capacities—210 cm^3/cm^3 in Pb-DOBDC and 0.18 g/g in PCN-11—at the same P_{max}. This trend toward reduced capacity extends to higher pressures of P_{max} = 65 and 100 bar, where the largest usable volumetric capacities are respectively 28 and 18% smaller than the largest total capacities at the equivalent P_{max}.

As P_{max} increases, the identity of the best-performing MOFs also changes. In particular, MOF-5 emerges as the MOF having the best combination of usable gravimetric and volumetric PS capacity at pressures above approximately 50 bar. The calculated capacity for MOF-5 is 168 cm^3 and 0.21 g/g at 65 bar and 203 cm^3/cm^3 and 0.25 g/g at 100 bar. This might come as a surprise given that MOF-5 has the *lowest* total volumetric capacity at these same P_{max} values. *This behavior highlights the pitfalls that may arise by focusing only on total, rather than on usable, capacity.* In our opinion, the reporting of usable capacities should be given a much higher priority. The reemergence of venerable MOF-5 as a high capacity adsorbent can be traced to the shape of its isotherm (Figure 6). Due to the absence of EBS, CH_4−MOF-5 interactions are relatively weak: ΔH = 12 kJ/mol.[18] Thus, the MOF-5 isotherm has a less pronounced slope at lower pressures, resulting in less retained CH_4 at 5 bar compared to the other MOFs. On the other hand, its slope is steepest at higher pressures, resulting in a more rapid increase in uptake with increasing pressure. Taken together, these observations suggest that EBS—due to their tendency to increase uptake at low pressures—can be *detrimental* at higher pressures for operating scenarios that employ an isothermal pressure swing. Figure S6 in the Supporting Information illustrates the crossover in CH_4 storage density for MOF-5 and PCN-11 as a function of P_{max}.

Usable Capacity: Temperature + Pressure Swing (TPS). Higher usable capacities can be achieved if desorption is triggered by a combined pressure and temperature swing. This operating scenario could be implemented using waste heat from combustion to warm the storage vessel during driving. The system would then be cooled at the forecourt during refueling. The benefits of this approach are illustrated in Figure 6c, which shows a reduction in the amount of residual CH_4 stored at 5 bar upon heating to 85 °C (358 K). (Our choice for this specific desorption temperature is motivated by the DOE requirement that the system temperature not exceed 358 K.)[4] Whether TPS operation would be advantageous will depend on the trade-off between higher CH_4 capacity versus the costs and efficiency losses associated with an in-tank heat exchanging system and additional cooling at the forecourt.

Table 3 demonstrates that TPS operation does in fact increase capacity beyond that of PS operation. For example, for

dx.doi.org/10.1021/jp4104273 | J. Phys. Chem. C 2014, 118, 2929−2942

P_{max} = 35 bar, Be-DOBDC is predicted to have the highest usable TPS capacity of 169 cm^3/cm^3. This is a 30% increase over the highest usable PS capacity (130 cm^3/cm^3 for PCN-11), yet remains 17% less than the total capacity of Be-DOBDC (204 cm^3/cm^3). At higher pressures the capacity advantage of TPS over PS diminishes: at 65 bar the capacities of the best-performing TPS MOFs are 17% larger than the best PS MOFs, and only 8% larger at 100 bar.

We note that the unfavorable performance associated with the EBS-MOFs under PS operation is minimized upon inclusion of a temperature swing. For example, Table 3 shows that Be- and Mg-DOBDC have among the highest TPS capacities at all values of P_{max}. This is of course due to the lower residual capacities present in these compounds at higher temperatures (Figure 6c) and suggests that EBS-MOFs can yield competitive capacities under TPS operation.

A summary of the best-performing MOFs and their respective capacities as a function of operating conditions is given in Table 4. (Here, "best-performing" refers to those MOFs that provide the best combination of volumetric and gravimetric capacity.) Of the 22 MOFs examined, Be-DOBDC, PCN-11, and MOF-5 emerge as the most promising methane adsorbents. Be-DOBDC and PCN-11 yield the best performance at low-to-moderate pressures of 35−65 bar, while MOF-5 is best at moderate-to-high pressures. To our knowledge Be-DOBDC has not yet been synthesized. However, given that the performance of well-known Mg-DOBDC is very similar to that of Be-DOBDC, one may substitute Mg for Be and achieve comparable properties.

Table 4. MOFs Exhibiting the Best Combination of Volumetric and Gravimetric CH_4 Density as a Function of Operating Conditions

operating condition, P_{max}	best MOF(s) (CH_4 capacity: cm^3/cm^3, g/g)
total, 35 bar	Be-DOBDC (204, 0.17)
total, 65 bar	Be-DOBDC (230, 0.20)
	PCN-11 (222, 0.22)
total, 100 bar	PCN-11 (244, 0.24)
	MOF-5 (225, 0.28)
usable PS, 35 bar	PCN-11 (130, 0.13)
usable PS, 65 bar	MOF-5 (168, 0.21)
usable PS, 100 bar	MOF-5 (203, 0.25)
usable TPS, 35 bar	Be-DOBDC (169, 0.15)
usable TPS, 65 bar	PCN-11 (198, 0.20)
usable TPS, 100 bar	MOF-5 (213, 0.27)

In addition to capacities, the thermal properties of the MOF can also impact performance. In particular, large enthalpies of adsorption (Figure 2) will generate greater cooling and heating loads during CH_4 uptake and release. These loads translate to higher costs and mass penalties associated with the heat exchanging subsystem in the storage vessel. As MOFs with EBS typically exhibit larger adsorption enthalpies—for example, ΔH ranges from 21 to 26 kJ/mol in Mg-DOBDC (ref 22 and Table 2) and is estimated at 15 kJ/mol in PCN-11[21]—we anticipate that these MOFs will be less desirable than MOF-5 (ΔH = 12 kJ/mol[18]) from a heat management standpoint.

We conclude our discussion by referring to Figure 8, which illustrates trends in gravimetric CH_4 capacity and pore volume versus MOF surface area.[68] Similar trends are well-known, for example, in the case of hydrogen storage in porous adsorbents;[67,69] a natural question is whether similar behavior holds for methane, as suggested by a few recent studies.[24,25,28] The existence of such trends would facilitate computational screening[70] based on simple geometric features such as surface area[68] and density. For the MOFs examined here, Figure 8 confirms that a strong linear correlation exists between surface area and either gravimetric capacity (Figure 8, left) or pore volume (Figure 8, right) across the M-DOBDC series. However, these correlations become less pronounced when the data set is expanded to include the higher-surface-area compounds (MOF-5, PCN-11, PCN-14, and HKUST-1). In these cases pore volume remains linearly correlated with surface area, but a similar trend is not observed for the gravimetric capacity. Measurements across a wider set of MOFs would be helpful in clarifying the generality of these trends. Additional analysis of correlations between CH_4 uptake and various MOF properties are presented in Figures S7 and S8 in the Supporting Information.

4. CONCLUSION

We have presented a computational study of the adsorption thermodynamics, electronic structure, and methane storage capacity in MOFs. Compounds examined include 18 metal-substituted variants of M-DOBDC, as well as several other prominent MOFs, including MOF-5, PCN-11/14, and HKUST-1. Important aspects of our study include (i) the benchmarking of van der Waals density functionals for prediction of ΔH, (ii) assessment of common interatomic

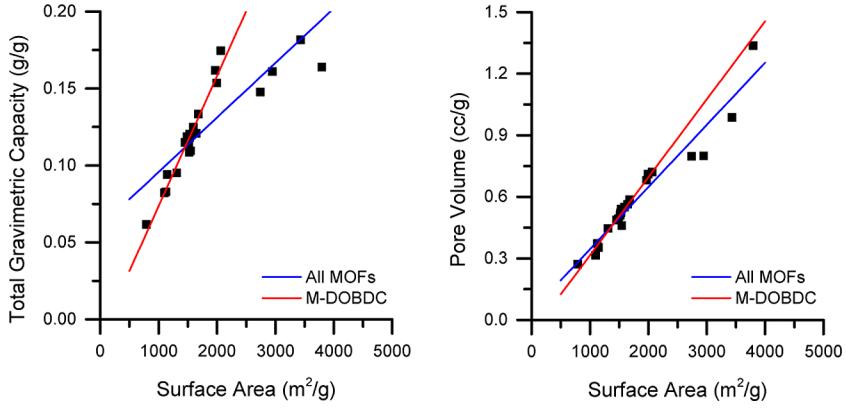

Figure 8. Relationship between surface area and (left) total gravimetric CH_4 capacity and (right) MOF pore volume in the M-DOBDC series (red line) and across all MOFs examined in this study (blue line) at P = 35 bar, T = 298 K.

dx.doi.org/10.1021/jp4104273 | J. Phys. Chem. C 2014, 118, 2929−2942

potentials for predicting CH_4 uptake, (iii) estimation of *usable* methane capacity under likely operating conditions, and (iv) clarification of the role of enhanced binding sites in CH_4 storage.

Regarding thermodynamic properties, methane adsorption enthalpies on the benchmark Mg- and Ni-DOBDC systems were calculated using several vdW-DFT methods and compared against experimental data. The vdW-DF2 scheme was found to yield the best agreement with experiments, with a small mean absolute deviation (MAD) of 3.7 kJ/mol. Applying this formalism across the entire M-DOBDC series, we observe that ΔH varies from −16 to −34 kJ/mol and weakly correlates with the ionic radius of the CUS. The calculated enthalpies are 10−20 kJ/mol less exothermic than for CO_2 adsorption in the same M-DOBDC compounds, suggesting that CH_4 adsorption in MOFs is dominated by weaker dispersion interactions. This assertion is supported by analysis of the charge density redistribution upon adsorption in Mg-DOBDC, which showed significantly less polarization in adsorbed CH_4 compared to prior studies on CO_2.

In addition to these thermodynamic analyses, CH_4 adsorption isotherms were evaluated using GCMC and compared against experimental data for nine prototype MOFs. The performance of six common interatomic potentials was critically assessed, taking into account variations in the description of the CH_4 molecule and the framework atoms. Of the various models considered, the uncharged, single-site TraPPE model for CH_4 in combination with a mixed DREIDING/UFF description for the MOF atoms yielded the best agreement with experiments, with a MAD of 15 cm^3/cm^3 at 298 K and pressures up to 35 bar.

The optimal potential was then used to predict the *usable* CH_4 capacities for isothermal pressure swing (PS) and temperature + pressure swing (TPS) operating scenarios. Significant differences exist between *total* capacities and less frequently reported *usable* capacities, with the usable capacities falling significantly below the (hypothetical) total capacities. We suggest that future studies of methane storage give less emphasis to total capacities in favor of reporting usable capacities, which should more closely resemble the performance of a realistic storage system. In our calculations Be-DOBDC, PCN-11, and MOF-5 emerge as the MOFs having the best combination of usable gravimetric and volumetric CH_4 densities. For pressure swing operation, PCN-11 yields the best performance at pressures below approximately 50 bar (130 cm^3/cm^3 and 0.13 g/g at 35 bar), while MOF-5 is best at higher pressures (168 cm^3/cm^3 and 0.21 g/g at 65 bar). Due to their tendency to retain CH_4 at low pressures, enhanced binding sites such as CUS or pocket sites are deemed to be detrimental for PS operation at higher pressures.

Other factors being equal, an optimal methane adsorbent should maximize capacity while minimizing thermal loads (i.e., minimize ΔH). Given its relatively low ΔH and high usable capacity, compounds analogous to MOF-5 are recommended for additional scrutiny as promising methane storage materials.

■ ASSOCIATED CONTENT

Supporting Information

Calculated binding energies (ΔE) and different energy components in ΔH, CH_4 geometrical parameters at adsorbed states, surface areas, pore volumes, isosteric heats of adsorption, and absolute uptake capacities (at 0.1, 35, and 100 bar) of M-DOBDC variants. This material is available free of charge via the Internet at http://pubs.acs.org.

■ AUTHOR INFORMATION

Corresponding Author

*E-mail: djsiege@umich.edu.

Notes

The authors declare no competing financial interest.

■ ACKNOWLEDGMENTS

We acknowledge helpful discussions with Dr. Jacob Goldsmith. H.Z. acknowledges financial support from the UM Summer Undergraduate Research Experience (SURE) program.

■ REFERENCES

(1) Burchell, T.; Rogers, M. Low Pressure Storage of Natural Gas for Vehicular Applications. *SAE Tech. Pap. Ser.* **2000**, *1*, 2205.
(2) Stephenson, J. *A Position Paper on Natural Gas Vehicles 1993*; International Association of NGVs: Auckland, New Zealand, 1993.
(3) 2009 Honda Civic GX Natural Gas Vehicle. http://automobiles.honda.com/civic-natural-gas/ (accessed 2013).
(4) ARPA-E. https://arpa-e-foa.energy.gov/ (accessed June 2012).
(5) NaturalGas.org. http://www.naturalgas.org/overview/background.asp (accessed June 2013).
(6) IOR Energy. http://web.archive.org/web/20100825042309/, http://www.ior.com.au/ecflist.html (accessed June 2013).
(7) Ferey, G. Hybrid Porous Solids: Past, Present, Future. *Chem. Soc. Rev.* **2008**, *37*, 191−214.
(8) Rowsell, J. L. C.; Yaghi, O. M. Metal−organic Frameworks: A new Class of Porous Materials. *Microporous Mesoporous Mater.* **2004**, *73*, 3−14.
(9) Long, J. R.; Yaghi, O. M. The Pervasive Chemistry of Metal-organic Frameworks. *Chem. Soc. Rev.* **2009**, *38*, 1213−1214.
(10) Morris, R. E.; Wheatley, P. S. Gas Storage in Nanoporous Materials. *Angew. Chem., Int. Ed.* **2008**, *47*, 4966−4981.
(11) Li, J.-R.; Kuppler, R. J.; Zhou, H.-C. Selective Gas Adsorption and Separation in Metal-organic frameworks. *Chem. Soc. Rev.* **2009**, *38*, 1477−1504.
(12) Murray, L. J.; Dinca, M.; Long, J. R. Hydrogen Storage in Metal-organic Frameworks. *Chem. Soc. Rev.* **2009**, *38*, 1294−1314.
(13) Li, J.-R.; Ma, Y.; McCarthy, M. C.; Sculley, J.; Yu, J.; Jeong, H.-K.; Balbuena, P. B.; Zhou, H.-C. Carbon Dioxide Capture-related Gas Adsorption and Separation in Metal-organic Frameworks. *Coord. Chem. Rev.* **2011**, *255*, 1791−1823.
(14) Düren, T.; Sarkisov, L.; Yaghi, O. M.; Snurr, R. Q. Design of New Materials for Methane Storage. *Langmuir* **2004**, *20*, 2683−2689.
(15) Ma, S.; Zhou, H.-C. Gas Storage in Porous Metal-organic Frameworks for Clean Energy Applications. *Chem. Commun.* **2010**, *46*, 44−53.
(16) Konstas, K.; Osl, T.; Yang, Y.; Batten, M.; Burke, N.; Hill, A. J.; Hill, M. R. Methane Storage in Metal Organic Frameworks. *J. Mater. Chem.* **2012**, *22*, 16698−16708.
(17) Eddaoudi, M.; Kim, J.; Rosi, N.; Vodak, D.; Wachter, J.; O'Keeffe, M.; Yaghi, O. M. Systematic Design of Pore Size and Functionality in Isoreticular MOFs and Their Application in Methane Storage. *Science* **2002**, *295*, 469−472.
(18) Zhou, W.; Wu, H.; Hartman, M. R.; Yildirim, T. Hydrogen and Methane Adsorption in Metal−Organic Frameworks: A High-Pressure Volumetric Study. *J. Phys. Chem. C* **2007**, *111*, 16131−16137.
(19) Makal, T. A.; Li, J.-R.; Lu, W.; Zhou, H.-C. Methane Storage in Advanced Porous Materials. *Chem. Soc. Rev.* **2012**, *41*, 7761−7779.
(20) Sculley, J.; Yuan, D.; Zhou, H.-C. The Current Status of Hydrogen Storage in Metal-organic Frameworks—updated. *Energy Environ. Sci.* **2011**, *4*, 2721−2735.
(21) Wang, X.-S.; Ma, S.; Rauch, K.; Simmons, J. M.; Yuan, D.; Wang, X.; Yildirim, T.; Cole, W. C.; López, J. J.; Meijere, A. d.; Zhou, H.-C. Metal−Organic Frameworks Based on Double-Bond-Coupled

Di-Isophthalate Linkers with High Hydrogen and Methane Uptakes. *Chem. Mater.* **2008**, *20*, 3145−3152.
(22) Wu, H.; Zhou, W.; Yildirim, T. High-Capacity Methane Storage in Metal−Organic Frameworks M2(dhtp): The Important Role of Open Metal Sites. *J. Am. Chem. Soc.* **2009**, *131*, 4995−5000.
(23) Dietzel, P. D. C.; Besikiotis, V.; Blom, R. Application of Metal-organic Frameworks with Coordinatively Unsaturated Metal Sites in Storage and Separation of Methane and Carbon Dioxide. *J. Mater. Chem.* **2009**, *19*, 7362−7370.
(24) Peng, Y.; Krungleviciute, V.; Eryazici, I.; Hupp, J. T.; Farha, O. K.; Yildirim, T. Methane Storage in Metal−Organic Frameworks: Current Records, Surprise Findings, and Challenges. *J. Am. Chem. Soc.* **2013**, *135*, 11887−11894.
(25) Wilmer, C. E.; Leaf, M.; Lee, C. Y.; Farha, O. K.; Hauser, B. G.; Hupp, J. T.; Snurr, R. Q. Large-scale Screening of Hypothetical Metal−organic Frameworks. *Nat. Chem.* **2012**, *4*, 83−89.
(26) Lin, X.; Telepeni, I.; Blake, A. J.; Dailly, A.; Brown, C. M.; Simmons, J. M.; Zoppi, M.; Walker, G. S.; Thomas, K. M.; Mays, T. J.; Hubberstey, P.; Champness, N. R.; Schröder, M. High Capacity Hydrogen Adsorption in Cu(II) Tetracarboxylate Framework Materials: The Role of Pore Size, Ligand Functionalization, and Exposed Metal Sites. *J. Am. Chem. Soc.* **2009**, *131*, 2159−2171.
(27) Ma, S.; Sun, D.; Simmons, J. M.; Collier, C. D.; Yuan, D.; Zhou, H.-C. Metal-Organic Framework from an Anthracene Derivative Containing Nanoscopic Cages Exhibiting High Methane Uptake. *J. Am. Chem. Soc.* **2007**, *130*, 1012−1016.
(28) Fernandez, M.; Woo, T. K.; Wilmer, C. E.; Snurr, R. Q. Large-Scale Quantitative Structure−Property Relationship (QSPR) Analysis of Methane Storage in Metal−Organic Frameworks. *J. Phys. Chem. C* **2013**, *117*, 7681−7689.
(29) He, Y.; Zhou, W.; Yildirim, T.; Chen, B. A Series of Metal-Organic Frameworks with high Methane Uptake and An Empirical Equation for Predicting Methane Storage Capacity. *Energy Environ. Sci.* **2013**, *6*, 2735−2744.
(30) Wu, H.; Simmons, J. M.; Liu, Y.; Brown, C. M.; Wang, X.-S.; Ma, S.; Peterson, V. K.; Southon, P. D.; Kepert, C. J.; Zhou, H.-C.; Yildirim, T.; Zhou, W. Metal−Organic Frameworks with Exceptionally High Methane Uptake: Where and How is Methane Stored? *Chem.—Eur. J.* **2010**, *16*, 5205−5214.
(31) Chen, L.; Morrison, C. A.; Düren, T. Improving Predictions of Gas Adsorption in Metal−Organic Frameworks with Coordinatively Unsaturated Metal Sites: Model Potentials, ab initio Parameterization, and GCMC Simulations. *J. Phys. Chem. C* **2012**, *116*, 18899−18909.
(32) Zhou, W. Methane Storage in Porous Metal−organic Frameworks: Current Records and Future Perspectives. *Chem. Rec.* **2010**, *10*, 200−204.
(33) Caskey, S. R.; Wong-Foy, A. G.; Matzger, A. J. Dramatic Tuning of Carbon Dioxide Uptake via Metal Substitution in a Coordination Polymer with Cylindrical Pores. *J. Am. Chem. Soc.* **2008**, *130*, 10870−10871.
(34) Koh, H. S.; Rana, M. K.; Hwang, J.; Siegel, D. J. Thermodynamic Screening of Metal-substituted MOFs for Carbon Capture. *Phys. Chem. Chem. Phys.* **2013**, *15*, 4573−4581.
(35) Socolow, R.; Desmond, M.; Aines, R.; Blackstock, J.; Bolland, O.; Kaarsberg, T.; Lewis, N.; Mazzotti, M.; Pfeffer, A.; Sawyer, K.; Siirola, J.; Smit, B.; Wilcox, J.*Direct Air Capture of CO_2 with Chemicals. A Technology Assessment for the APS Panel on Public Affairs*; American Physical Society: College Park, MD, 2011.
(36) Hohenberg, P.; Kohn, W. Inhomogeneous Electron Gas. *Phys. Rev.* **1964**, *136*, B864−B871.
(37) Yang, Q.; Zhong, C. Molecular Simulation of Carbon Dioxide/Methane/Hydrogen Mixture Adsorption in Metal−Organic Frameworks. *J. Phys. Chem. B* **2006**, *110*, 17776−17783.
(38) Grimme, S. Semiempirical GGA-type Density Functional Constructed with a Long-range Dispersion Correction. *J. Comput. Chem.* **2006**, *27*, 1787−1799.
(39) Dion, M.; Rydberg, H.; Schröder, E.; Langreth, D. C.; Lundqvist, B. I. Van der Waals Density Functional for General Geometries. *Phys. Rev. Lett.* **2004**, *92*, 246401.
(40) Chen, L.; Grajciar, L.; Nachtigall, P.; Düren, T. Accurate Prediction of Methane Adsorption in a Metal−Organic Framework with Unsaturated Metal Sites by Direct Implementation of an ab Initio Derived Potential Energy Surface in GCMC Simulation. *J. Phys. Chem. C* **2011**, *115*, 23074−23080.
(41) Lee, K.; Murray, É. D.; Kong, L.; Lundqvist, B. I.; Langreth, D. C. Higher-accuracy van der Waals Density Functional. *Phys. Rev. B* **2010**, *82*, 081101.
(42) Kong, L.; Cooper, V. R.; Nijem, N.; Li, K.; Li, J.; Chabal, Y. J.; Langreth, D. C. Theoretical and Experimental Analysis of H_2 binding in a Prototypical Metal-organic Framework Material. *Phys. Rev. B* **2009**, *79*, 081407.
(43) Rana, M. K.; Koh, H. S.; Hwang, J.; Siegel, D. J. Comparing van der Waals Density Functionals for CO_2 Adsorption in Metal Organic Frameworks. *J. Phys. Chem. C* **2012**, *116*, 16957−16968.
(44) Park, J.; Kim, H.; Han, S. S.; Jung, Y. Tuning Metal−Organic Frameworks with Open-Metal Sites and Its Origin for Enhancing CO_2 Affinity by Metal Substitution. *J. Phys. Chem. Lett.* **2012**, *3*, 826−829.
(45) Canepa, P.; Arter, C. A.; Conwill, E. M.; Johnson, D. H.; Shoemaker, B. A.; Soliman, K. Z.; Thonhauser, T. High-throughput Screening of Small-molecule Adsorption in MOF. *J. Mater. Chem. A* **2013**, *1*, 13597−13604.
(46) Perdew, J. P.; Burke, K.; Ernzerhof, M. Generalized Gradient Approximation Made Simple. *Phys. Rev. Lett.* **1996**, *77*, 3865.
(47) Karra, J. R.; Walton, K. S. Effect of Open Metal Sites on Adsorption of Polar and Nonpolar Molecules in Metal−Organic Framework Cu-BTC. *Langmuir* **2008**, *24*, 8620−8626.
(48) Martin, M. G.; Siepmann, J. I. Transferable Potentials for Phase Equilibria. 1. United-Atom Description of n-Alkanes. *J. Phys. Chem. B* **1998**, *102*, 2569−2577.
(49) Chen, B.; Siepmann, J. I. Transferable Potentials for Phase Equilibria. 3. Explicit-Hydrogen Description of Normal Alkanes. *J. Phys. Chem. B* **1999**, *103*, 5370−5379.
(50) Sun, Y.; Spellmeyer, D.; Pearlman, D. A.; Kollman, P. Simulation of the Solvation Free Energies for Methane, Ethane, and Propane and Corresponding Amino Acid Dipeptides: A Critical Test of the Bond-PMF Correction, A new Set of Hydrocarbon Parameters, and the Gas Phase-water Hydrophobicity Scale. *J. Am. Chem. Soc.* **1992**, *114*, 6798−6801.
(51) Lucena, S. M. P.; Frutuoso, L. F. A.; Silvino, P. F. G.; Azevedo, D. C. S.; Toso, J. P.; Zgrablich, G.; Cavalcante, C. L., Jr. Molecular Simulation of Collection of Methane Isotherms in Carbon Material using all-atom and United Atom Models. *Colloids Surf., A* **2010**, *357*, 53−60.
(52) Rappe, A. K.; Casewit, C. J.; Colwell, K. S.; Goddard, W. A.; Skiff, W. M. UFF, a Full Periodic Table Force Field for Molecular Mechanics and Molecular Dynamics Simulations. *J. Am. Chem. Soc.* **1992**, *114*, 10024−10035.
(53) Mayo, S. L.; Olafson, B. D.; Goddard, W. A. DREIDING: A Generic Force Field for Molecular Simulations. *J. Phys. Chem.* **1990**, *94*, 8897−8909.
(54) Kresse, G.; Furthmüller, J. Efficient Iterative Schemes for Ab initio Total-energy Calculations using a Plane-wave Basis Set. *Phys. Rev. B* **1996**, *54*, 11169−11186.
(55) Blöchl, P. E. Projector Augmented-wave Method. *Phys. Rev. B* **1994**, *50*, 17953−17979.
(56) Canepa, P.; Chabal, Y. J.; Thonhauser, T. When Metal Organic Frameworks Turn into Linear Magnets. *Phys. Rev. B* **2013**, *87*, 094407.
(57) Bloch, E. D.; Queen, W. L.; Krishna, R.; Zadrozny, J. M.; Brown, C. M.; Long, J. R. Hydrocarbon Separations in a Metal-Organic Framework with Open Iron(II) Coordination Sites. *Science* **2012**, *335*, 1606−1610.
(58) Campañá, C.; Mussard, B.; Woo, T. K. Electrostatic Potential Derived Atomic Charges for Periodic Systems Using a Modified Error Functional. *J. Chem. Theory Comput.* **2009**, *5*, 2866−2878.
(59) Spek, A. Single-crystal Structure Validation with the Program PLATON. *J. Appl. Crystallogr.* **2003**, *36*, 7−13.
(60) Klimeš, J.; Bowler, D. R.; Michaelides, A. Van der Waals Density Functionals Applied to Solids. *Phys. Rev. B* **2011**, *83*, 195131.

(61) Klimeš, J.; Bowler, D. R.; Michaelides, A. Chemical Accuracy for the Van der Waals Density Functional. *J. Phys.: Condens. Matter* **2010**, *22*, 022201.
(62) Sillar, K.; Sauer, J. Ab Initio Prediction of Adsorption Isotherms for Small Molecules in Metal−Organic Frameworks: The Effect of Lateral Interactions for Methane/CPO-27-Mg. *J. Am. Chem. Soc.* **2012**, *134*, 18354−18365.
(63) Wang, S. Comparative Molecular Simulation Study of Methane Adsorption in Metal−Organic Frameworks. *Energy Fuels* **2007**, *21*, 953−956.
(64) Lucena, S. M. P.; Mileo, P. G. M.; Silvino, P. F. G.; Cavalcante, C. L. Unusual Adsorption Site Behavior in PCN-14 Metal−Organic Framework Predicted from Monte Carlo Simulation. *J. Am. Chem. Soc.* **2011**, *133*, 19282−19285.
(65) Getzschmann, J.; Senkovska, I.; Wallacher, D.; Tovar, M.; Fairen-Jimenez, D.; Düren, T.; van Baten, J. M.; Krishna, R.; Kaskel, S. Methane Storage Mechanism in the Metal-organic Framework Cu3(btc)2: An in Situ Neutron Diffraction Study. *Microporous Mesoporous Mater.* **2010**, *136*, 50−58.
(66) Senkovska, I.; Kaskel, S. High Pressure Methane Adsorption in the Metal-organic Frameworks Cu3(btc)2, Zn2(bdc)2dabco, and Cr3F(H2O)2O(bdc)3. *Microporous Mesoporous Mater.* **2008**, *112*, 108−115.
(67) Moellmer, J.; Moeller, A.; Dreisbach, F.; Glaeser, R.; Staudt, R. High Pressure Adsorption of Hydrogen, Nitrogen, Carbon Dioxide and Methane on the Metal−organic Framework HKUST-1. *Microporous Mesoporous Mater.* **2011**, *138*, 140−148.
(68) Frost, H.; Düren, T.; Snurr, R. Q. Effects of Surface Area, Free Volume, and Heat of Adsorption on Hydrogen Uptake in Metal−Organic Frameworks. *J. Phys. Chem. B* **2006**, *110*, 9565−9570.
(69) Rouquerol, F.; Rouquerol, J.; Sing, K. Introduction. In *Adsorption by Powders and Porous Solids*; Academic Press: London, 1999; Chapter 1, pp 1−26.
(70) Panella, B.; Hirscher, M.; Roth, S. Hydrogen adsorption in different carbon nanostructures. *Carbon* **2005**, *43*, 2209−2214.